

NUMERICAL DRAG AND LIFT PREDICTION FRAMEWORK FOR SUPERELLIPSOIDAL PARTICLES IN MULTIPHASE FLOWS

MITJA ŠTRAKL¹, JANA WEDEL², PAUL STEINMANN^{2,3}, MATJAZH HRIBERŠEK¹ & JURE RAVNIK¹

¹ Faculty of Mechanical Engineering, University of Maribor, Slovenia.

² Institute of Applied Mechanics, University of Erlangen-Nürnberg, Germany.

³ Glasgow Computational Engineering Center, University of Glasgow.

ABSTRACT

The numerical treatment of industrial and environmental problems, involving multiphase flows with particles, has gained significant interest of researchers over the recent years. For large-scale problems, involving an increased number of particles, authors mostly rely on the Lagrangian particle tracking approach, where particle-fluid interaction is generally unresolved and has to be modelled. Significant research efforts have already been made in developing various models to predict particle-fluid interaction, where applications involving complex particle shapes are especially intriguing. In the majority of encountered problems, particle dynamics is primarily governed by drag forces exerted on the particle by the carrier fluid. Following from that it is unsurprising that precise particle trajectories can only be established from accurate particle drag prediction model. In this context, we present a steady-state particle-resolved numerical model, based on OpenFOAM, for numerical drag prediction of superellipsoidal particles in Stokesian flow regime. The idea behind particle-resolved model is to benefit from multi parameter drag prediction, which considers not only the flow regime and particle size but also detailed geometric features (expressed by four independent parameters) and particle orientation. The proposed numerical model will also benefit from a parametric geometry formulation, which will allow to evaluate the drag force for the entire range of particle shapes, offered by the superellipsoidal parametrization. For a vast amount of non-spherical particles, this significantly improves the accuracy of the predicted drag force in comparison to traditional drag models, which do not account for the entire range of influencing factors. The numerical model is further supported by an automated parametric mesh generation algorithm, which makes it possible to autonomously address the full range of particle orientations in parallel. The parametric algorithm also enables the specification of various flow regimes, which are captured in the analysis. Thus, with a single set of input parameters, one can quickly obtain the drag function for given particle shape, with respect to the entire range of orientations and flow regimes. The authors believe that the proposed solution will significantly reduce the effort to obtain an accurate drag model for a vast amount of non-spherical particle shapes.

Keywords: computational fluid dynamics, drag, Lagrangian particle tracking, lift, multiphase flow, superellipsoid.

1 INTRODUCTION

Scientific analyses of particle-laden flows are nowadays conducted worldwide, considering various problems in natural sciences and industrial applications. Authors have extensively relied on the assumption of spherical particle shape for years, for which the expressions of aerodynamic forces [1–3] are well established in the entire range of flow regimes. Significant research interest still exists for this approach, as there were many applications in recent time [4, 5], where a sphere is in fact the closest approximation of the actual particle geometry. On the other hand, there are several problems, where the particle shape is distinctively non-spherical, so their trajectories can therefore not be captured with reasonable accuracy by spherical fluid dynamic models. Unlike for spheres, a single, universal

approach to model fluid dynamic forces on non-spherical particles does not exist. Historically, numerous efforts have been made to overcome this difficulty, which eventually led to a few different approaches, with respect to problem nature, that are predominantly used today. For the vast majority of problems where very small particles are encountered, relative particle-fluid interaction usually remains in the creeping flow regime, where fluid dynamic forces can be predicted by a few readily available analytical models, derived for a limited selection of non-spherical particles, like prolate spheroids [6] or ellipsoids [7]. The latter model was successfully employed by various authors, to study the dynamics of non-spherical particles in flows, such as fibres [8, 9] and disks [10]. However, this relatively straightforward approach lacks the prediction capabilities when creeping flow limits are exceeded, in terms of particle Reynolds number Re_p , which is exactly the case in numerous studies, where larger and heavier particles are considered. Due to the increased particle response time (Stokes number $St \gg 1$), it is not uncommon in such flows that Re_p approaches the order of magnitude of 10, or even 100 [11], where flow separation occurs, possibly extending into the turbulent regime. To capture fluid dynamic forces in such regimes, an experimental or numerical approach is necessary. The latter became popular in recent years, when already established models for non-spherical shapes, like ellipsoids and fibres, were extended to moderate [12, 13] or large [14] Reynolds numbers. Extensions were also made to include different particle shapes like cylinders [15] and other irregular non-distinctive shapes [16]. Despite the substantial benefits in terms of accuracy, such an approach is rarely used, when specific particle shapes need to be captured, due to increased efforts required to produce the results for all flow regimes and all non-symmetrical particle orientations. In this fashion, a few generalized approaches have been proposed, based on the generalization of the particle shape [17], in terms of sphericity $\psi = A_s/A$ and the volume equivalent diameter $d_p = (6V_p/\pi)^{1/3}$. While such an approach offers significant simplification for the formulation and generally yields reasonable prediction accuracy, it is far from ideal. Two of its main drawbacks are the loss of shape information and the lack of orientation consideration, which makes this approach appropriate mainly for sphere-like geometries. As emphasized by many authors so far [13, 18], an accurate prediction of fluid forces exerted on a particle is of essential importance for predicting the trajectories and obtaining other information relevant to the study. That said, an extension of readily available models to other similar shapes would be highly beneficial, to reduce the gap between shape specific models, which offer a superior accuracy and generalized ones that can process a wider range of shapes, but at the cost of accuracy. In this fashion, we propose an extension to the existing fluid dynamic force model for ellipsoids, by introducing superellipsoidal formulation, which expands the parametrization capabilities to significantly wider range of shapes, i.e. cylinders and cuboids. Additionally, we are presenting the numerical framework, used to capture the fluid forces in various flow regimes and all non-symmetrical particle orientations, based on automated design of experiments generation.

2 NUMERICAL FRAMEWORK

In this study, we aim to examine fluid dynamic forces acting on non-spherical particles in incompressible fluid flow. We consider a complete, three-dimensional numerical approach, to allow for the treatment of arbitrary particle shapes and a possible extension to flows with moderate Reynolds numbers, where axial symmetry of the flow pattern is lost. To obtain a

comprehensive overview of drag and lift distribution on an arbitrary non-spherical particle, fluid forces must be captured for wider ranges of Reynolds numbers and for the entire range of non-symmetrical particle orientations. For this reason, we propose a numerical model of incompressible fluid flow around a particle, by the way of an automated generation of design of experiments (DoE).

2.1 Numerical fluid flow formulation

The governing equations of the incompressible viscous motion of a Newtonian fluid are given by:

$$\begin{aligned} \frac{\partial \mathbf{u}}{\partial t} + \mathbf{u} \cdot \nabla \mathbf{u} &= \mathbf{g} - \frac{1}{\rho} \nabla p + \nu \nabla^2 \mathbf{u} \\ \nabla \cdot \mathbf{u} &= 0, \end{aligned} \quad (1)$$

where p , ρ , \mathbf{u} are pressure, fluid density and fluid velocity, \mathbf{g} represents gravity and ν is the fluid kinematic viscosity. Discretization of (1) and numerical computation are performed in a finite volume framework – OpenFOAM – using its incompressible transient solver `pisoFoam`, based on the PISO algorithm. For the present study, solver settings are configured so that the turbulent stress term is omitted, since our main interest remains in flows with lower relative Reynolds number $Re_p = |\mathbf{u}_p - \mathbf{u}| d_p / \nu$, where \mathbf{u}_p is the particle velocity and d_p is the volume equivalent sphere diameter. We are searching for a geometry parametrization technique such that a single parametric equation could handle a vast amount of particle shapes that are often encountered in particulate flows. A significant research interest already exists for ellipsoidal particles, so the next reasonable step would be an extension of this formulation. Thus, we choose a superellipsoidal parametrization, which is given by

$$P(x, y, z) = \left(\left| \frac{x}{a} \right|^{2/e_2} + \left| \frac{y}{b} \right|^{2/e_2} \right)^{e_2/e_1} + \left| \frac{z}{c} \right|^{2/e_1}, \quad (2)$$

where a , b , c are superellipsoid x , y , z half-axes, respectively, while e_1 and e_2 are its exponent parameters. The superellipsoid volume is determined by the following expression:

$$V_p = 2abce_1 e_2 B\left(\frac{e_1}{2} + 1, e_1\right) B\left(\frac{e_2}{2}, \frac{e_2}{2}\right), \quad (3)$$

where $B(x, y)$ is the beta function, which is related to the gamma function Γ by the expression $B(x, y) = \Gamma(x)\Gamma(y)/\Gamma(x+y)$. Following from momentum conservation law in continuum mechanics, fluid forces, exerted on the particle surface area, are obtained by direct integration of the pressure and viscous stresses from the flow field,

$$\mathbf{F} = - \int_A p \cdot \mathbf{n} dA + \rho \nu \int_A \left[\nabla \mathbf{u} + (\nabla \mathbf{u})^T \right] \cdot \mathbf{n} dA. \quad (4)$$

In the present numerical setting, the only non-zero velocity component is $\mathbf{u} = u_0 \hat{\mathbf{i}}$. This in turn allows us to express the drag and lift components of the above given force in principal

components of the global frame, which yields $F_D = |F_x \hat{i}|$ and $F_L = |F_y \hat{j} + F_z \hat{k}|$, for drag and lift respectively. In this formulation, lift is expressed by the $L2$ -norm of the two force components that are perpendicular to the velocity vector. While such an approach lacks the directional information (important for non-axisymmetric bodies), it is beneficial for introducing the drag and lift coefficients, which are expressed by the particle equivalent sphere diameter, namely

$$Cd = \frac{8F_D}{\rho \pi d_p^2 |\mathbf{u}|^2}, Cl = \frac{8F_L}{\rho \pi d_p^2 |\mathbf{u}|^2}. \quad (5)$$

2.2 Numerical framework validation

Special consideration was given to properly sizing the domain, since we aim to allow for the treatment of various flow regimes. Some authors have already established that applications with extremely low-Re flows can be particularly demanding when it comes to domain sizing. This follows from the fact that in such cases the main mechanism of momentum transport is by diffusion, which in theory has an infinite reach (when $Re \rightarrow 0$). By reviewing the works of other authors (related to our application), we detected significant discrepancies at employing the computational domain, in terms of shape and size. Chadil et al. [19], for example, used a rectangular domain of $16d_p \times 8d_p$ in their DNS model of flow around a sphere, similar to Zastawny et al. [13], who employed a domain of $20d_p \times 20d_p \times 10d_p$ for their IBM setup for non-spherical particles. Andersson and Jiang [20] performed an extensive domain study for low-Re flow around non-spherical particles, where the domain measure is given as a volume equivalent cube edge length. They examined edge lengths from $20d_p$ to $170d_p$ and reported that the domain independent solution was obtained at around $135d_p$. In the present study, the numerical domain configuration (Fig. 1) is employed in similar fashion to traditional studies of external aerodynamics, by positioning the particle body in the centre of the rectangular flow field domain, bounded by planar surfaces, representing the far-field boundaries. A Dirichlet boundary condition is used to set inlet velocity to a fixed value ($u = u_0 i$), the particle

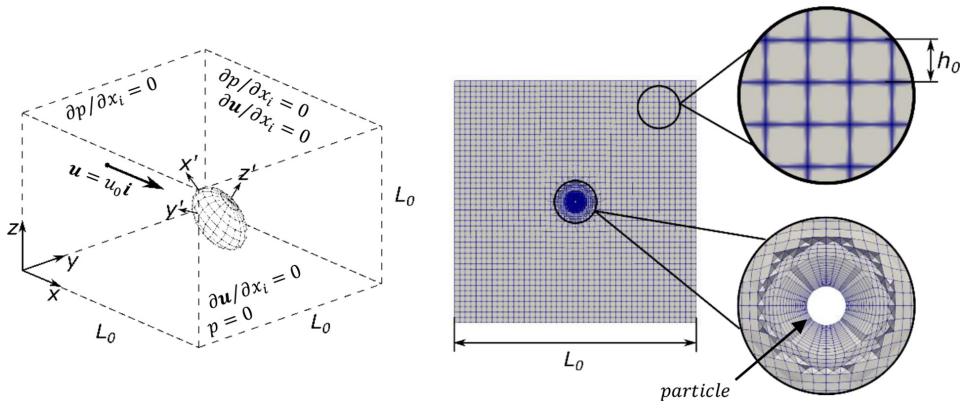


Figure 1: Numerical domain sizing and configuration, including boundary conditions (left), with centre cross-section view of the computational mesh (case D3/M3) and highlighted mesh areas of interest (right).

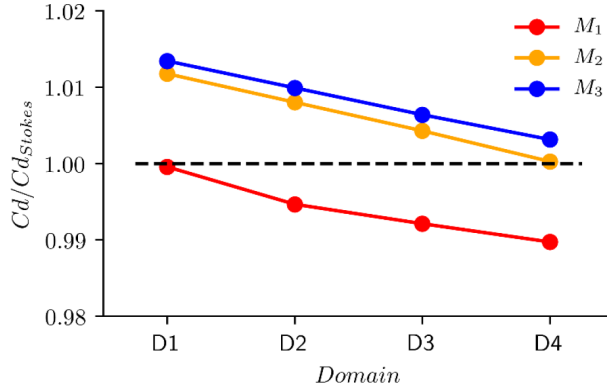


Figure 2: Resulting drag coefficients of a sphere in a Stokes flow with $Re = 10^{-3}$ are presented. Data are displayed for all configurations from Table 1, where each line represents a single mesh density across all domains.

wall velocity to zero and pressure at the outlet to zero, while a Neumann boundary condition is employed for the velocity ($\partial u / \partial x_i = 0$) on other domain boundaries and for the pressure at the inlet ($\partial p / \partial x_i = 0$). We examined four different domain sizes, with edge lengths L_0 in the range from $80d_p$ to $240d_p$ and three different meshes, with base element edge lengths h_0 from $8d_p$ to $2.7d_p$, as presented in Table 1. This reflects the size of the far-field elements, whereas elements near the particle surface are refined by the ratio of 2^7 . All refinement ratios are kept constant between the meshes, only the base element edge length was altered.

A domain and mesh study is performed by setting up a reference case of flow around a sphere with $Re = 10^{-3}$. Since we are presenting a numerical model for fluid forces calculation, we use the drag coefficient Cd as a measure for validation, where Stokes drag is used as a reference. Results are displayed in Fig. 2 in terms of the ratio of calculated drag coefficient over Stokes drag coefficient for considered Reynolds number. As indicated in the figure, we establish that an insufficient domain size tends to overpredict the drag, whereas an insufficient mesh resolution leads to its underprediction. This is also the most probable cause for the ‘spot-on’ match with Stokes drag in case of D1/M1, where it appears that the two errors have cancelled out. In an overall assessment, we conclude that all configurations yield satisfactory results. For further investigations, we decide to use the configuration D3/M1, as using the configurations from the lower right section of Table 1 cannot be justified by their negligibly superior accuracy. One could even consider case D1/M1 acceptable, but when migrating to a non-spherical geometry, the lack of domain span could have an increased influence on the

Table 1: Number of mesh elements for domain configurations D1 to D4 and mesh densities M1 to M3.

Mesh (h_0)	Domain (L_0)			
	D1 ($80d_p$)	D2 ($120d_p$)	D3 ($160d_p$)	D4 ($240d_p$)
M1 ($8d_p$)	9,448	11,830	16,448	35,448
M2 ($4d_p$)	54,544	79,470	110,544	272,601
M3 ($2.7d_p$)	171,910	258,036	360,910	873,910

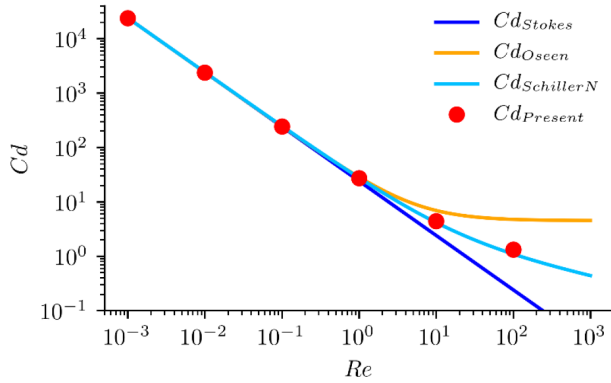


Figure 3: Drag coefficients of a sphere in the extended range of Re numbers are displayed, in comparison with Stokes analytical drag and with other well-established empirical models (Schiller-Naumann [3], Oseen [2]) that have been extensively used for years.

results, since the flow pattern around the particle would change due to its geometry and orientation. To evaluate the entire numerical framework, together with the selected domain and mesh configuration (D3/M1), we extend the scope of investigations to the spherical reference case with higher Reynolds numbers, as presented in Fig. 3. The present drag coefficients are best matched by Schiller-Naumann [3] empirical correlation, which is valid for Re numbers up to 800 [17]. The relative error of present results, compared to the Schiller-Naumann model, is kept below 2% in Stokes flow regime, while it increases to about 10% approaching the maximum tested Reynolds number of 100.

This increase of relative error is probably caused by the mesh resolution, which might be slightly too coarse, to capture the smallest flow structures that start to occur at higher Reynolds number. Nevertheless, the overall accuracy is satisfactory and the model is considered validated within the range of tested flow regimes.

2.3 Design of numerical experiments

Our main objective is to study fluid dynamic drag and lift properties of specific shape particles, taking into account the entire range of non-symmetric orientations. Since the effort of manually generating the required number of numerical experiments is considerable, we decide to automate this process in order to keep this routine in timely manner. Using the parametric equation (2), one can introduce the extension to ellipsoidal geometry and obtain shapes like cylinders, cuboids, rhomboids and even octahedrons, as indicated in Fig. 4. Since we are considering non-spherical particles, particle orientation, with respect to the flow field, must be expressed. The traditional fashion of establishing a single angle of incidence would not be sufficient for arbitrary non-axisymmetric bodies, as they experience different forces with respect to the angle of ‘drag-lift’ plane. Thus, we establish a two-angle (φ and θ) definition for the direction of the velocity vector, relative to the particle local frame, in somehow similar fashion to spherical coordinates (Fig. 5).

Following from eq. (2), one can establish that the resulting surface exhibits planar symmetry for all principal planes. This leads to the conclusion that the range of non-symmetrical orientations spans from 0° to 90° for both, φ and θ , while the rest of orientations can be

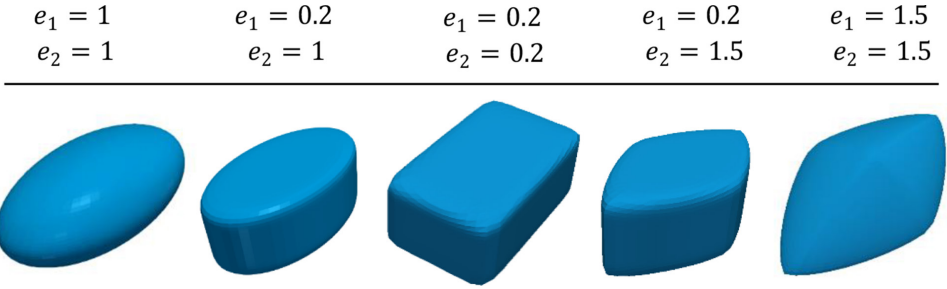


Figure 4: Examples of superellipsoidal particles. The first from the left is a triaxial ellipsoid, while the following four are oval cylinder, cuboid, rhomboid and octahedron. All examples are formed from the same axes (a, b, c), by only altering the exponential parameters (e_1, e_2).

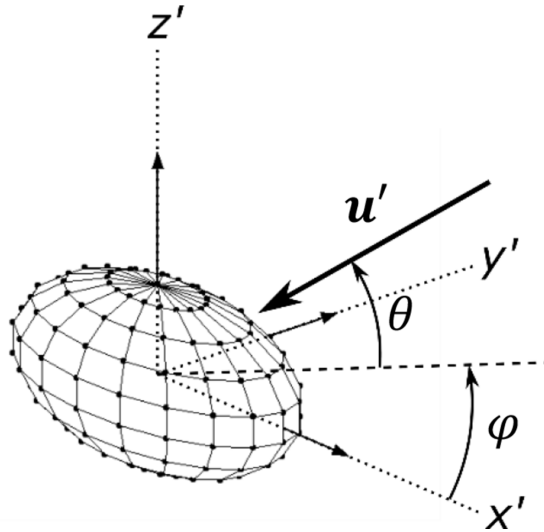


Figure 5: Definition of the velocity vector, relative to the particle local frame, by two orientation angles (φ and θ).

covered by simply mirroring the results across all principal planes. To account for the range of particle orientations that need to be examined, we define a rotational formalism, which is used to transform the geometry to arbitrary orientations, with respect to the flow field. A rotation matrix \underline{R} is employed, based on the local frame (x', y', z') direction cosines, which are expressed in terms of Euler parameters (q_0, q_1, q_2, q_3).

3 RESULTS

3.1 Flow around a prolate ellipsoid

A prolate ellipsoid particle was generated, according to eq. (2), by setting $a = 2.5$ and keeping the rest of the parameters at unity. Numerical simulation was employed in the Stokes flow regime at $Re = 10^{-2}$, using the presented numerical framework. A study of all non-symmetrical orientations has been performed, by using the presented DoE generator. Since the prolate

ellipsoid is an axisymmetric body, the range of non-symmetrical orientations is reduced to a single plane, with its normal perpendicular to the semi minor half axis of the ellipsoid. This in turn means that only a single angle (φ) can be used to describe the range of orientations, which goes from 0° to 90° . This approach was employed to generate the reduced number of DoE cases, for which fluid forces were computed as given by eq. (4). Following from that, drag and lift coefficients were derived by eq. (5), which are displayed in Fig. 6 and compared to Brenner’s [7] analytical formulation. This comparison is provided to further support the validity of the presented numerical model, by including the non-spherical case with different orientations.

Two straightforward conclusions can be drawn from the figure, the first is that the maximum drag is formed when the projected area is the greatest, which is at $\varphi = 90^\circ$, and the second is that the maximum lift occurs at $\varphi = 45^\circ$. This is only possible at very low Reynolds numbers, where the flow stays attached across the entire surface. Any other way, as soon as some separation would begin to occur, it would promote the formation of a stall when further increasing the incidence angle. The magnitude of the total fluid dynamic force, exerted on this ellipsoid, is not very different from that exerted on a sphere. For this ellipsoid, two no-lift orientations exist, where the minimum (at $\varphi = 0^\circ$) and maximum (at $\varphi = 90^\circ$) total force magnitude is exerted on the particle.

3.2 Flow around a triaxial ellipsoid

A triaxial ellipsoid was generated, using the parameters $a = 2.5, b = 1.5, c = 1, e_1 = 1, e_2 = 1$. Contrary to the prolate ellipsoid, a triaxial ellipsoid does not exhibit axial symmetry, which in turn means that the range of non-symmetrical orientations would have to be defined by two angles, as presented in the second half of section 2.3 and displayed in Fig. 5. Other than that, the process of setting up a fluid dynamic study was analogous to prolate ellipsoid case. An identical flow regime, with $Re = 10^{-2}$, was established, and drag and lift coefficients were computed. The coefficients are presented on Fig. 7, in the form of a product with Re number. Within the limits of Stokes flow, this can be assumed as a measure of drag and lift, related only to the particle geometry, so it can be applied to any Re number within this regime.

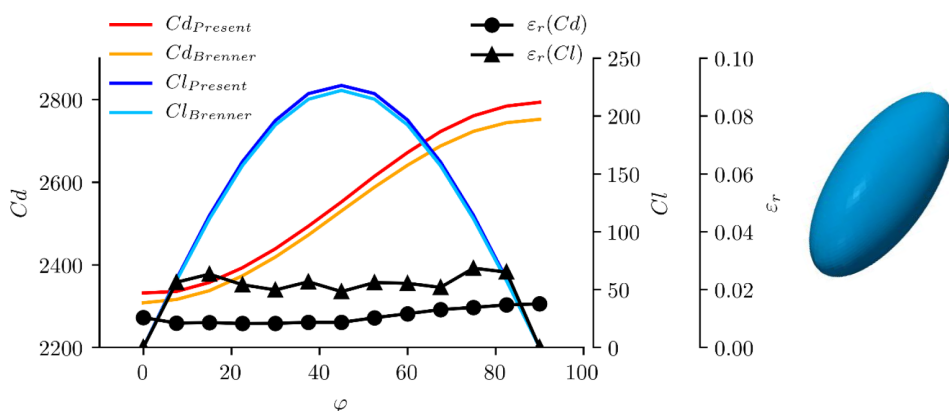


Figure 6: Drag and lift coefficients of a prolate ellipsoid in Stokes flow with $Re = 10^{-2}$ are displayed in range of φ from 0° to 90° . Three y-axes are established on this plot, where left is used for drag scale, first right for lift scale and second right for relative error scale.

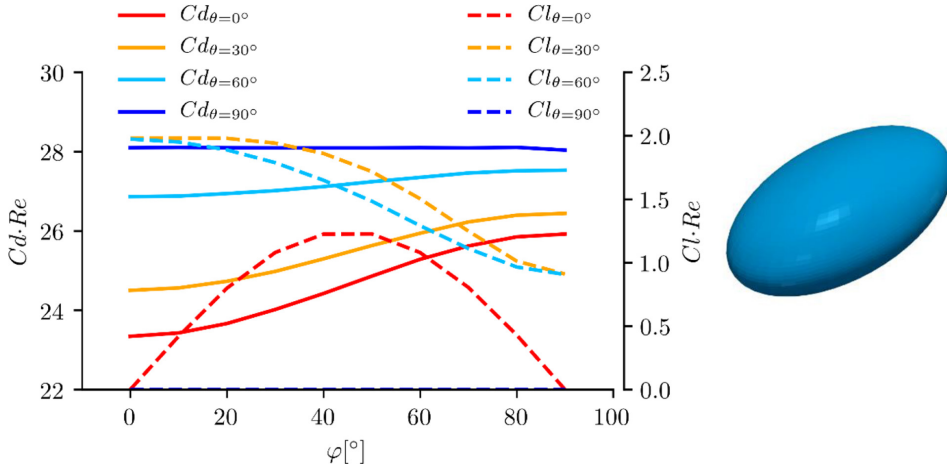


Figure 7: Drag and lift coefficients of a triaxial ellipsoid in Stokes flow. Simulation was performed at $Re = 10^{-2}$. Drag and lift products with the Re number are displayed on the left- and right-hand y-axes respectively. Rotation angle φ is plotted on the x-axis, while θ is presented in steps by four different lines, as indicated on a chart legend. The rightmost side of the figure represents the considered particle shape.

As evident from Fig. 7, the drag and lift coefficients are influenced by both orientation angles, which demonstrates the lack of axisymmetric properties of this geometry. The minimal drag is obtained in zero-lift case where φ and θ are both 0° , while the maximum drag occurs at the total zero-lift case, at $\theta = 90^\circ$, where drag is constant and lift is zero across the entire range of φ . This is a special case among all non-symmetrical orientations, where the velocity vector is aligned with the particle local z-axis, which causes that φ rotations are limited to the plane, perpendicular to the flow and thus have no effect on the resulting drag and lift values. Setting the angle to $\varphi = 0^\circ$ and $\theta = 45^\circ$, one obtains maximum lift, which reflects the particle axial ratios, namely $a > b > c$. Following from that, one can also establish that variations of both, drag and lift, are most pronounced by fixing φ to 0° and altering θ . Due to axial ratios, this configuration causes the greatest change in the projected area.

3.3 Flow around an oval disk

In order to demonstrate the functionality of the proposed superellipsoidal parametrization, another fluid dynamic study was employed, on a representative case of this geometrical group. An oval disk-like particle was introduced, defined by the following parameter set: $a = 2.5$, $b = 1.5$, $c = 1$, $e_1 = 0.2$, $e_2 = 1$. The rest of the setup was employed using the same approach as with the triaxial ellipsoid case, with results presented in Fig. 8.

By comparing the results with the former case, similar conclusion can be drawn regarding the orientations of minimal and maximal drag and lift. This is not surprising, as some resemblance still exists between the particles, namely the axial ratios are the same. The magnitude of maximal drag is almost identical, while minimal drag is somewhat higher as with the triaxial ellipsoid, which is not surprising, considering the ‘shaper’ edges of a superellipsoid. As for the lift, it is slightly lower in magnitude for all configurations and it is less varied between the minimum and maximum lift orientations. Overall, the general fluid dynamic impression is similar to the triaxial ellipsoid; however, the two are fairly distinct from the prolate-ellip-

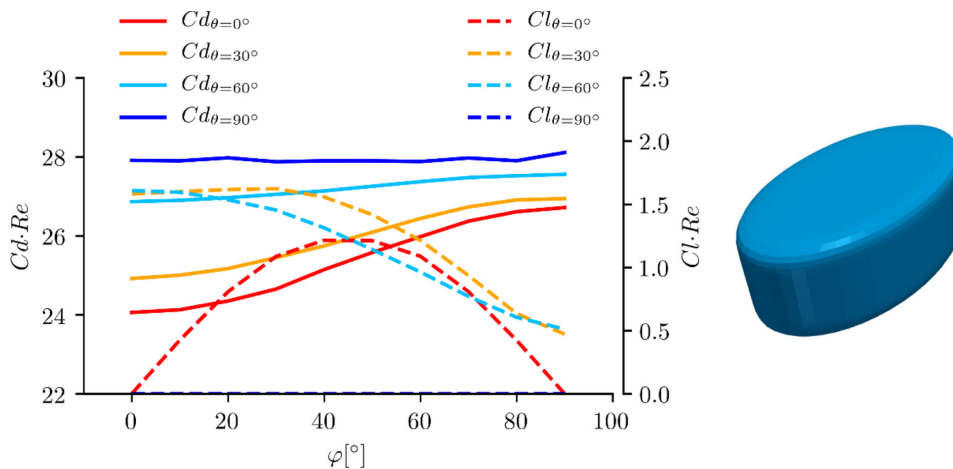


Figure 8: Drag and lift coefficients of an oval disk in Stokes flow. Simulation was performed at $Re = 10^{-2}$. Drag and lift products with Re number are displayed on left- and right-hand y-axes respectively. Rotation angle φ is plotted on the x-axis, while θ is presented in steps by four different lines, as indicated on a chart legend. The rightmost side of the figure represents the considered particle shape.

solid case, where axial symmetry allows for substantially simplified treatment (as orientations are distributed on a single plane).

4 CONCLUSION

A numerical framework for drag and lift force modelling on superellipsoidal particles is proposed. The idea behind this model is to provide a relatively straightforward solution to obtaining the drag and lift forces for superellipsoidal particles in multiphase flows. An automated DoE generation is introduced, based on the superellipsoidal parametric equation, which allows for the geometry definition by only four parameters. Since the particles are non-spherical, rotational formalisms are established to allow for the treatment of arbitrary orientations. Using this approach, a DoE generator creates the entire range of non-symmetrical particle orientations with pre-defined discrete steps, so that drag and lift distributions can be obtained. The setup of the numerical configuration, together with domain size and mesh resolution analysis, was evaluated and substantiated in the process of numerical framework validation. After that, the proposed framework was validated on a spherical example, where wider range of flow regimes was examined and results were compared to well-known empirical correlations for spherical drag. That said, the numerical framework functionality was demonstrated on three examples, namely a prolate ellipsoid, a triaxial ellipsoid and an oval disk-like superellipsoid. All of the examples were subjected to the simulated Stokes flow environment, and drag and lift correlations were established. The results of all considered particles were presented, whereby most notable differences between the particles were pointed out. A triaxial ellipsoid and superellipsoid were found to behave quite similar in terms of drag magnitude and distribution, while for the lift, some differences were observed at the force distribution as well as the magnitude. On the other hand, we detected significant deviation between the axisymmetric and non-axisymmetric particles, where for the latter, the drag and lift analysis was proven to be substantially more demanding, due to three-dimensional properties of force formation.

ACKNOWLEDGEMENT

The authors thank the Deutsche Forschungsgemeinschaft for the financial support in the framework of the project STE 544/58.

REFERENCES

- [1] Stokes, G.G., On the effect of the internal friction of fluids on the motion of pendulums. *Transactions of Cambridge Philosophical Society*, **9**, p. 8, 1851.
- [2] Oseen, C.W., *Neuere Methoden und Ergebnisse in der Hydrodynamik*. Akad. Verlagsgesellschaft, Leipzig, 1927.
- [3] Schiller, L. & Naumann, A., Über die grundlegenden Berechnungen bei der Schwerkraftaufbereitung. *VDI*, **77(12)**, pp. 318–320, 1933. <https://doi.org/10.1007/bf01611926>
- [4] Wedel, J., Steinmann, P., Štrakl, M., Hriberšek, M. & Ravnik, J., Can CFD establish a connection to a milder COVID-19 disease in younger people? Aerosol deposition in lungs of different age groups based on Lagrangian particle tracking in turbulent flow. *Computational Mechanics*, **67(5)**, pp. 1497–1513, March 2021. <https://doi.org/10.1007/s00466-021-01988-5>
- [5] Koullapis, P., et al., Regional aerosol deposition in the human airways: The SimInhale benchmark case and a critical assessment of in silico methods. *European Journal of Pharmaceutical Sciences*, **113**, pp. 77–94, February 2018. <https://doi.org/10.1016/j.ejps.2017.09.003>
- [6] Happel, J. & Brenner, H., *Low Reynolds number hydrodynamics*, vol. 1. Englewood Cliffs: Prentice-Hall, 1965.
- [7] Brenner, H., The Stokes resistance of an arbitrary particle-III. Shear fields. *Chemical Engineering Science*, **19(9)**, pp. 631–651, September 1964. [https://doi.org/10.1016/0009-2509\(64\)85052-1](https://doi.org/10.1016/0009-2509(64)85052-1)
- [8] Ravnik, J., Marchioli, C., Hriberšek, M. & Soldati, A., On shear lift force modelling for non-spherical particles in turbulent flows. *AIP Conference Proceedings*, **1558**, pp. 1107–1110, 2013. <https://doi.org/10.1063/1.4825700>
- [9] Dotto, D., Soldati, A. & Marchioli, C., Deformation of flexible fibers in turbulent channel flow. *Meccanica*, **55(2)**, pp. 343–356, February 2020. <https://doi.org/10.1007/s11012-019-01074-4>
- [10] Yuan, W., Andersson, H.I., Zhao, L., Challabotla, N.R. & Deng, J., Dynamics of disk-like particles in turbulent vertical channel flow. *International Journal of Multiphase Flow*, **96**, pp. 86–100, November 2017. <https://doi.org/10.1016/j.ijmultiphaseflow.2017.06.008>
- [11] Cui, K.F.E., Zhou, G.G.D., Jing, L., Chen, X. & Song, D., Generalized friction and dilatancy laws for immersed granular flows consisting of large and small particles. *Physics of Fluids*, **32(11)**, p. 113312, November 2020. <https://doi.org/10.1063/5.0024762>
- [12] Ouchene, R., Khalij, M., Tanière, A. & Arcen, B., Drag, lift and torque coefficients for ellipsoidal particles: From low to moderate particle Reynolds numbers. *Computers & Fluids*, **113**, pp. 53–64, 2015. <https://doi.org/10.1016/j.compfluid.2014.12.005>
- [13] Zastawny, M., Mallouppas, G., Zhao, F. & van Wachem, B., Derivation of drag and lift force and torque coefficients for non-spherical particles in flows. *International Journal of Multiphase Flow*, **39**, pp. 227–239, March 2012. <https://doi.org/10.1016/j.ijmultiphaseflow.2011.09.004>
- [14] Ouchene, R., Khalij, M., Arcen, B. & Tanière, A., A new set of correlations of drag, lift and torque coefficients for non-spherical particles and large Reynolds numbers.

- Powder Technology*, **303**, pp. 33–43, December 2016. <https://doi.org/10.1016/j.powtec.2016.07.067>
- [15] Guo, X., Lin, J. & Nie, D., New formula for drag coefficient of cylindrical particles. *Particology*, **9(2)**, pp. 114–120, April 2011. <https://doi.org/10.1016/j.partic.2010.07.027>
- [16] Sun, Q., Zhao, G., Peng, W., Wang, J., Jiang, Y. & Yu, S., Numerical predictions of the drag coefficients of irregular particles in an HTGR. *Annals of Nuclear Energy*, **115**, pp. 195–208, May 2018. <https://doi.org/10.1016/j.anucene.2018.01.040>
- [17] Crowe, C.T., Schwarzkopf, J.D., Sommerfeld, M. & Tsui, Y., *Multiphase flows with droplets and particles: Second edition*. New York: CRC Press, 2011.
- [18] Castang, C., Laín, S. & Sommerfeld, M., Pressure center determination for regularly shaped non-spherical particles at intermediate Reynolds number range. *International Journal of Multiphase Flow*, **137**, p. 103565, April 2021. <https://doi.org/10.1016/j.ijmultiphaseflow.2021.103565>
- [19] Chadil, M.A., Vincent, S. & Estivalèzes, J.L., Accurate estimate of drag forces using particle-resolved direct numerical simulations. *Acta Mechanica*, **230(2)**, pp. 569–595, February 2019. <https://doi.org/10.1007/s00707-018-2305-1>
- [20] Andersson, H.I. & Jiang, F., Forces and torques on a prolate spheroid: low-Reynolds-number and attack angle effects. *Acta Mechanica*, **230(2)**, pp. 431–447, February 2019. <https://doi.org/10.1007/s00707-018-2325-x>